Journal of Sound and Vibration 328 (2009) 191–202

Contents lists available at ScienceDirect

Journal of Sound and Vibration

journal homepage: www.elsevier.com/locate/jsvi

An alternative Poincaré section for high-order harmonic and chaotic responses of a rubbing rotor

Jang-Der Jeng [a], Yuan Kang [b,*], Yeon-Pun Chang [b]

[a] Department of Mechanical Engineering, National United University, Taiwan, ROC
[b] Department of Mechanical Engineering, Chung Yuan Christian University, Taiwan, ROC

ARTICLE INFO

Article history:
Received 27 June 2008
Received in revised form
27 June 2009
Accepted 21 July 2009
Handling Editor: L.G. Tham
Available online 22 August 2009

ABSTRACT

A rotor system in rubbing is shown to exhibit complex phenomena including higher subharmonic oscillation, period-doubling bifurcation and chaotic motions due to its strongly nonlinear dynamic characteristics. This study introduces an alternative Poincaré section method to analyze the dynamic behavior of a rotor in rubbing. This response integration for analyzing high-order harmonic and chaotic responses is used to integrate the distance between state trajectory and the origin in the phase plane during a specific period. This integration process is based on the fact that the integration value would be constant if the integration interval is equal to the response period. It provides a quantitative characterization of system responses and can assist the role of the traditional stroboscopic technique (Poincaré section method) to observe bifurcations and chaos of the nonlinear oscillators. For a rubbing rotor the response composes of multiple high-order harmonic motions or chaos with extreme contamination, which cannot be easily to be distinguished either from orbit plot or from Poincaré map. Combining the capability of precisely identifying period and constructing bifurcation diagrams, the advantages of the proposed method are shown by simulations.

1. Introduction

Considering the needs of high rotating speed and high efficiency in the modern machines, the decreasing clearance between the rotor and the stator is a necessary design. The Rub-impact between rotor and stator can be one of the main malfunctions which often occur in rotating machinery. It is mainly resulted from the mass imbalance, turbine, compressor blade failure, defective bearing, or rotor misalignment. A faulty rotor is generally associated with a vibrating system having complicated nonlinear behavior. Regarding some types of faults, the vibration of system contains a very complicated phenomenon including not only the periodic motion but also the chaotic motion. In the rotor systems with different types of faults, a detailed investigation on various forms of vibrations is of great importance to establish a reliable diagnosis system for the rotating machinery. When a rub-impact happens, the partial rub arises at first. During a complete period, the rub and impact interactions occur between the rotor and stator once or fewer times. Gradual deterioration of the partial rub will lead to the full rub and then the vibration will affect the normal operation of the machines severely.

The majority of works was focused on the development of some mathematical models; this is in order to make the rubbing phenomenon more accurately to be understood in the past few decades. A rotor system with rub-impact is

* Corresponding author. Tel.: +886 3 2654315; fax: +886 3 2654351.
E-mail address: yk@cycu.edu.tw (Y. Kang).

0022-460X/$ - see front matter © 2009 Elsevier Ltd. All rights reserved.
doi:10.1016/j.jsv.2009.07.018

Nomenclature

K	nondimensional stiffness ratio; $K = k/k_s$	ΔX	initial horizontal eccentric ratio; $\Delta X = \Delta x/\delta$
F_N, F_T	radial impact, tangential rubbing forces	ΔY	initial vertical eccentric ratio; $\Delta Y = \Delta y/\delta$
F_x, F_y	rub-impacting force in the x and y directions	c	damping of the shaft
O	geometric center of end bearing	k	stiffness of the shaft
O_S	center of the stator	k_s	stiffness of the stator
P_T	response integration value for T ($T = 2\pi/\Omega$)	r	radial displacement of the rotor
P_{nT}	response integration value for nT	τ_c	nondimensional arbitrary extraction time
R	nondimensional radial displacement of the rotor; $R = r/\delta$	x	displacement of the rotor in the horizontal direction
U	nondimensional imbalance; $U = mu/M\delta$	y	displacement of the rotor in the vertical direction
X	nondimensional displacement of the rotor in the horizontal direction; $X = x/\delta$	δ	radial clearance between rotor and stator
Y	nondimensional displacement of the rotor in the horizontal direction; $Y = y/\delta$	μ	friction coefficient between rotor and stator
Ω	nondimensional rotating speed of the rotor; $\Omega = \omega/\omega_n$	τ	nondimensional time; $\tau = \omega_n t$
		ω	rotating speed of the rotor
		ω_n	natural frequency of the rotor; $\omega_n = \sqrt{k/M}$
		ξ	non-dimensional damping of the rotor; $\xi = c/2\sqrt{kM}$

considered as importance in several of practical engineering fields. There have been numerous publications launched on this topic. In particular, Childs [1,2], Beatty [3], Choy [4] and Choi [5] paid attention to the dynamic phenomena in rotating machinery with rotor-to-stator contact.

Beatty [3] proposed a mathematical model for rubbing forces and a detailed response format of diagnostic data in actual cases. The model is still applied widely today. A comprehensive investigation on the dynamic characteristics exhibited by this kind of system is necessary in order to diagnose this fault. Choy [4] performed a very interesting theoretical investigation to observe the effects of casing stiffness, friction coefficient, imbalance load, system damping on rub force history, and the transient response of rotor orbit; but only periodic vibration was discussed. Choi [5] examined the complex dynamic behavior of a simple horizontal Jeffcott rotor with bearing clearances. Numerical results have revealed the alternating periodic. He proposed a numerical method which combined the harmonic balance method with discrete Fourier transformation and inverse discrete Fourier transformation. Their numerical results show the occurrence of super and subharmonics located in a rotor model involved a bearing clearance.

Ehrich [6,7] addressed the subject of higher subharmonic response for high-speed rotor in bearing clearance. He used a modified Jeffcott model to analyze the subharmonic vibration and also performed a series of numerical simulations under various conditions of rotating speed, damping and stiffness ratio in order to examine the behavior of the system. He concluded that the sub-critical super-harmonic response is the exact opposite of the super-critical subharmonic response. Goldman [8,9] applied an analytical approach associated with the numerical calculation to study the phenomenon with supercritical subharmonic for a rotor system with clearance. The results showed regular periodic vibrations of synchronous and subharmonic order, as well as chaotic vibration patterns of the rotor, all accompanied by higher harmonic motion. Chu [10,11] performed a numerical investigation to observe periodic, quasi-periodic and chaotic motions in a rub-impact rotor system which is supported on the oil film bearings. Routes into and out of chaos were analyzed. They discussed a nonlinear vibration of the Jeffcott rotor system which includes a nonlinear rub-impact forces resulted from the eccentric rotation of rotor. The analytical expression of the stable periodic solution is obtained by using the Fourier serious expansion method. They found that whenever the rub-impact occurs, three kinds of routes into the chaos will arise as the rotating speed increases. Through a period of doubling bifurcation, these phenomena from a stable periodic motion graze bifurcation as a chaos, and then a sudden transition happened between the periodic vibration and chaos.

Edwards [12] investigated the torsion effect included in a contacting rotor-stator system. They also examined the system's response regarding the torsional stiffness, and concluded that torsion has a substantial effect on system response. Feng [13] discussed the vibration phenomena in rotor-stator contact which is caused by an initial perturbation. The perturbation is an instantaneous change of the radial velocity when the rotor is rotating in its normal steady state. Being under certain conditions, they found that the rotor will remain rubbing with the stator, even if the initial perturbation no longer exists.

The dynamic behavior of rotor system with rubbing was investigated by several researchers. The published literatures have mainly qualitative characters. In the present study, to the author's knowledge, the quantitative observation for the high-order harmonic and chaotic responses of a rubbing rotor system has not been studied in the literature. The integration algorithm is proposed to analyze the responses of the rotor system with rub-impact. With applying this method, this is able to assist the role of Poincaré section points in the process of constructing bifurcation diagram. Some case simulations are given here to illustrate its effectiveness and convenience.

2. Rotor model and motion equation

The model utilized in this work is based on a Jeffcott rotor as shown in Fig. 1. It is assumed that a rotor mounted on a flexible, isotropic shaft and simply supported by bearings at both ends. The weight of the rotor and shaft acts as a gravitational force which is supported by bearing force due to its stationary eccentricity. The force equilibrium of rotor in whirling with rub-impact is shown in Fig. 2. O_s is the center of the stator and O is the geometric center of end bearing.

An initial clearance of δ is installed between rotor and stator. When rubbing between rotor and stator occurs occasionally, the elastic impact must be induced. Also, Coulomb friction between both contact surfaces is assumed. The radial component due to impact is denoted by F_N and the tangential component due to friction is denoted by F_T which can be determined by

$$F_N = \begin{cases} 0 & (r-\delta)<0 \\ k_s(r-\delta) & (r-\delta)\geq 0 \end{cases} \tag{1a}$$

and

$$F_T = \mu F_N \tag{1b}$$

where k_s is the stiffness of the stator; μ is the friction coefficient between rotor and stator, r is the radial displacement of the rotor which can be expressed as $r=\sqrt{(x-\Delta x)^2+(y-\Delta y)^2}$. Δx and Δy are the initial eccentric distances in x and y directions. It indicates that whenever the radial displacement of rotor is smaller than the static clearance between rotor and stator, there will be no rub-impact; and the rub-impacting forces will be absent.

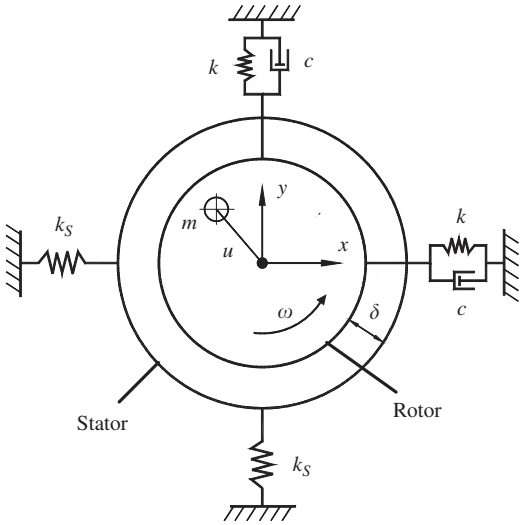

Fig. 1. Schematic of the rotor with damping and stiffness.

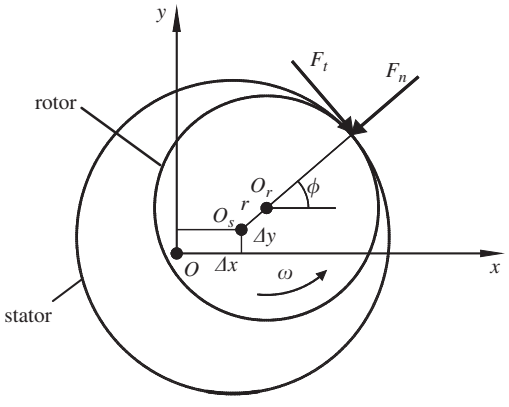

Fig. 2. Rub-impacting rotor system.

The above normal and tangential forces can be transformed in both x and y directions to give two forces $F_x(x,y)$ and $F_y(x,y)$ as follows:

$$\begin{cases} F_x(x,y) = -F_N \cos\phi + F_T \sin\phi \\ F_y(x,y) = -F_N \sin\phi - F_T \cos\phi \end{cases} \tag{2}$$

or

$$\begin{bmatrix} F_x \\ F_y \end{bmatrix} = \frac{k_s(r-\delta)}{r} \begin{bmatrix} -1 & \mu \\ -\mu & -1 \end{bmatrix} \begin{bmatrix} (x-\Delta x) \\ (y-\Delta y) \end{bmatrix} H(r-\delta) \tag{3}$$

where

$$H(r-\delta) = \begin{cases} 0 & (r-\delta)<0 \\ 1 & (r-\delta) \geq 0 \end{cases}$$

$\cos\phi = (x-\Delta x)/r$ and $\sin\phi = (y-\Delta y)/r$.

The differential motion equations for the rotor with rub-impact can be described in x–y coordinates as

$$M\ddot{x} + c\dot{x} + kx = mu\omega^2 \cos(\omega t) + F_x \tag{4a}$$

$$M\ddot{y} + c\dot{y} + ky = mu\omega^2 \sin(\omega t) + F_y \tag{4b}$$

where M is the mass of shaft and rotor, c and k are the damping and the stiffness of the shaft, respectively, ω is the rotating speed.

The equations of motion were nondimensionalized in order to transform the system into the dimensionless domain, in which the responses of different physical systems can be conveniently compared. The dimensionless variables and parameters are as follows:

$$X = x/\delta, \quad Y = y/\delta, \quad \omega_n = \sqrt{k/M}, \quad \Omega = \omega/\omega_n, \quad \tau = \omega_n t, \quad \xi = c/2\sqrt{k\mathrm{M}}$$
$$U = mu/M\delta, \quad K = k/k_s, \quad R = r/\delta$$

Then, the dimensionless motion equations of the rub-impacting rotor system can be expressed as

$$X'' + 2\xi X' + X = U\Omega^2 \cos(\Omega\tau) - (1/K)(1-1/R)\{X-\mu Y\}H(R-1) \tag{5}$$

$$Y'' + 2\xi Y' + Y = U\Omega^2 \sin(\Omega\tau) - (1/K)(1-1/R)(\mu X + Y)H(R-1) \tag{6}$$

where the prime indicates the time derivative with respect to τ and

$$H(R-1) = \begin{cases} 0 & (R-1)<0 \\ 1 & (R-1) \geq 0 \end{cases}$$

If no rubbing occurs ($R<1$), the governing equations of motion can be formulated as

$$X'' + 2\xi X' + X = U\Omega^2 \cos(\Omega\tau) \tag{7}$$

$$Y'' + 2\xi Y' + Y = U\Omega^2 \sin(\Omega\tau) \tag{8}$$

It indicates that whenever the radial displacement of rotor is smaller than the static clearance between rotor and stator, there will be no rub-impact; and the rub-impacting forces will be absent.

3. Method of integration algorithm

An algorithm, denoted by P_{nT}, was defined by integrating the distance of rotor trajectories and the origin in phase plane as can be expressed by

$$P_{nT}(\tau_c) = \int_{\tau_c}^{\tau_c+nT} ([X(\tau)]^2 + [Y(\tau)]^2)^{1/2}\,\mathrm{d}\tau \tag{9}$$

where n is an integer, $X(\tau)$ and $Y(\tau)$ are the displacement components of rotor center in X and Y directions, respectively, τ_c is an initial time which is chosen arbitrarily only when the response of rotor system reaches steady state. The integration interval nT, where the T is the period of single excitation or the smallest common multiple period of multiple excitations, is set to be the predicted, confirmed, oscillating period. When P_{nT} $(n=1)$ is a constant, the system response is P–1 periodic motion. Therefore, when the integration interval is set at nT (n is an integer larger than zero), it can be judged that the system periodic response is P–n motion, that is, the n-th is a sub-harmonic response. Therefore, when the integration interval is set at nT (n is an integer larger than zero), it can be judged that the system periodic response is P–n motion, that

is, the n-th is a subharmonic response. Moreover, if the integration interval is set as the excitation period, i.e., T, the results can be used to draw the bifurcation diagram of the rotor system. The extraction period is the same as Poincaré section method.

When the rotor system steady response is in the integration interval nT, it is periodic motion. The response integration algorithm is demonstrated as the following:

$$f(X,Y) = f(X(\tau + nT), Y(\tau + nT)) \tag{10}$$

Note that $f(X,Y)$ is the right-hand of a resultant first-order differential equation. Eq. (9) is differentiated by time τ_c. From the above formula, the following is obtained:

$$\begin{aligned}\frac{dP_{nT}(\tau_c)}{d\tau_c} &= f(X(\tau_c + nT)), Y(\tau_c + nT)) - f(X(\tau_c), Y(\tau_c)) \\ &= f(X(\tau + nT), Y(\tau + nT)) - f(X(\tau), Y(\tau)) = 0\end{aligned} \tag{11}$$

Therefore,

$$P_{nT}(\tau_c) = \text{constant} \tag{12}$$

It should be noted that the above procedure is structured on the basis that the integral value P_{nT} would be constant as opposed to varied starting times τ_c, if the chosen integration interval nT is equal to the response period. Another point addressed is that the period is determined on the basis that the P_{nT} value remains constant over τ_c This avoids possible error, by measurement or computation tolerance, occurring in the process of distinguishing the geometric points of Poincaré section in phase space. Furthermore, by utilizing the method of P_{nT} integration mentioned above, the set of simulated or experimental data needed to determine response period all reside in the time range $[\tau_c, \tau_c + nT + \Delta\tau_c]$, the duration of which is $(nT + \Delta\tau_c)$. With the freedom to set $\Delta\tau_c$ small, the duration $(nT + \Delta\tau_c)$ is less than nTs, which is usually the time span utilized by the Poincaré section to collect data for identifying response period due to measurement or numerical tolerance. Therefore, when limited experimental measurement data are analyzed, it is more advantageous to use the response integration method.

4. Simulation results and analysis

Due to the strongly nonlinear characteristics of the rub-impacting rotor system, the vibration responses are quite complicated. It is difficult to obtain the exact solutions directly. For this reason, the derived above equations of motion are first transferred into a set of first-order differential equations. Then the equations are solved by the fourth-order Runge–Kutta method to obtain data. During the calculation a smaller integration step has to be chosen to ensure a stable solution and to avoid the numerical divergence at the point where derivatives of the rub-impact forces are discontinuous.

4.1. Comparisons with integration and Poincaré section methods

The rotating speed is one of the most important parameters affecting the dynamic characteristics of a rotor system. Figs. 3–8 show the response integration value plots and Poincaré maps with various rotating speed ratios, Ω of 2.34, 2.368, 2.48, 2.68, 2.7925 and 2.8, respectively, where $K = 0.015$, $\xi = 0.068$, $\Delta X = 0.3$, $\Delta Y = 0.92$, $U = 0.1$, $\mu = 0.2$. In the analysis of the Poincaré section method, the extraction time equals to the external excitation period of $T = 2\pi/\Omega$. At $\Omega = 2.34$, there are three isolated points in the Poincaré map as shown in Fig. 3(b). The result of the response integration method also shows the motion to be period three as shown in Fig. 3(a). At $\Omega = 2.368$, due to a few Poincaré section points being too

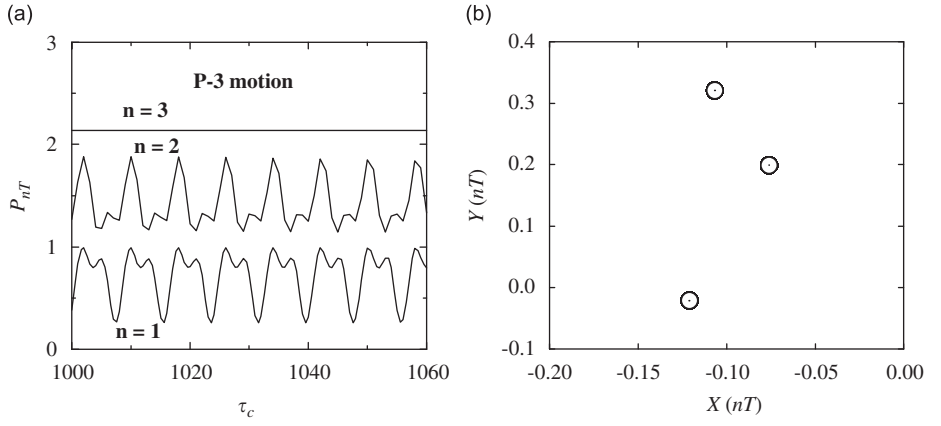

Fig. 3. (a) The response integration value plot and (b) Poincaré map with rotating speed ratio, $\Omega = 2.34$.

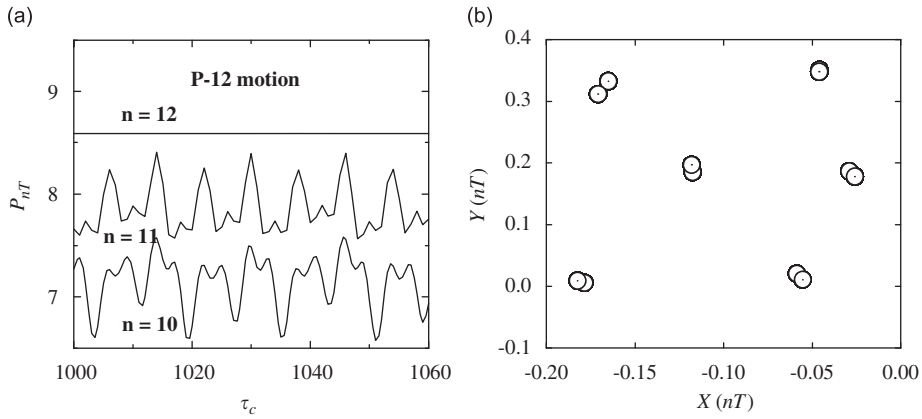

Fig. 4. (a) The response integration value plot and (b) Poincaré map with rotating speed ratio, $\Omega = 2.368$.

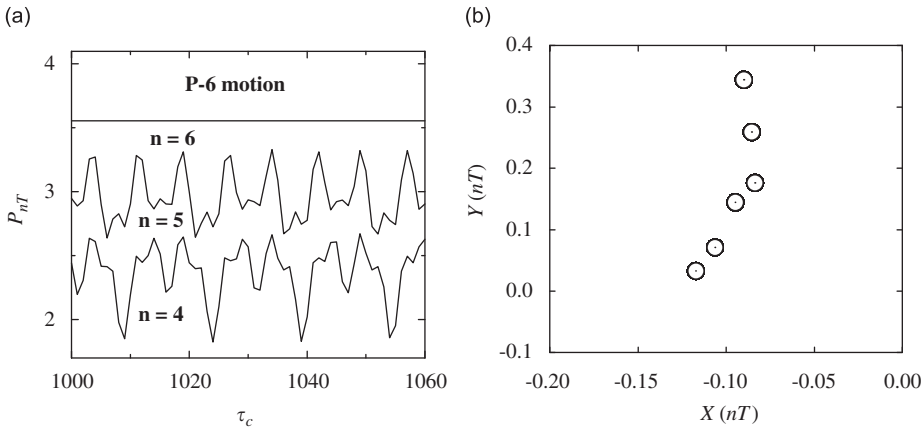

Fig. 5. (a) The response integration value plot and (b) Poincaré map with rotating speed ratio, $\Omega = 2.48$.

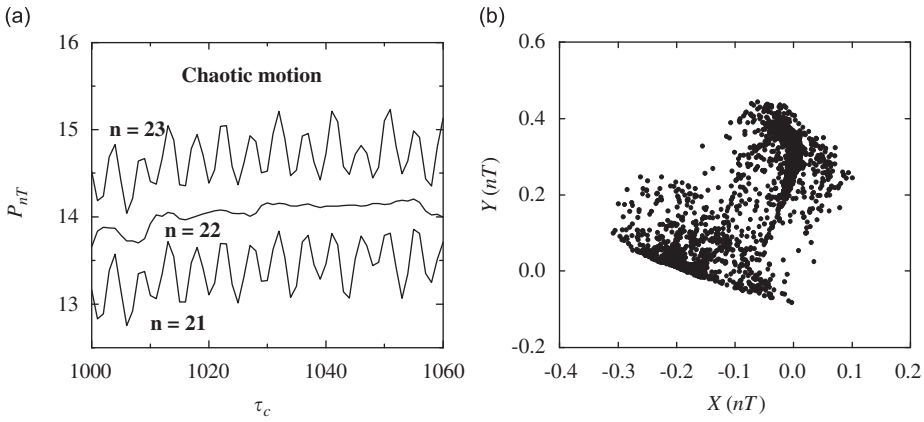

Fig. 6. (a) The response integration value plot and (b) Poincaré map with rotating speed ratio, $\Omega = 2.68$.

close, it is difficult to identify the periodic response of the sub-harmonic vibration as shown in Fig. 4(b). But from Fig. 4(a), the response integration value plot, we can differentiate the motion clearly to be a sub-harmonic vibration with period 12. When the rotating speed ratio is 2.48, the motion is regular and periodic as the orbit map. There is still six points in the Poincaré map. Also, the response integration value plot, we can clearly differentiate the motion to be a sub-harmonic

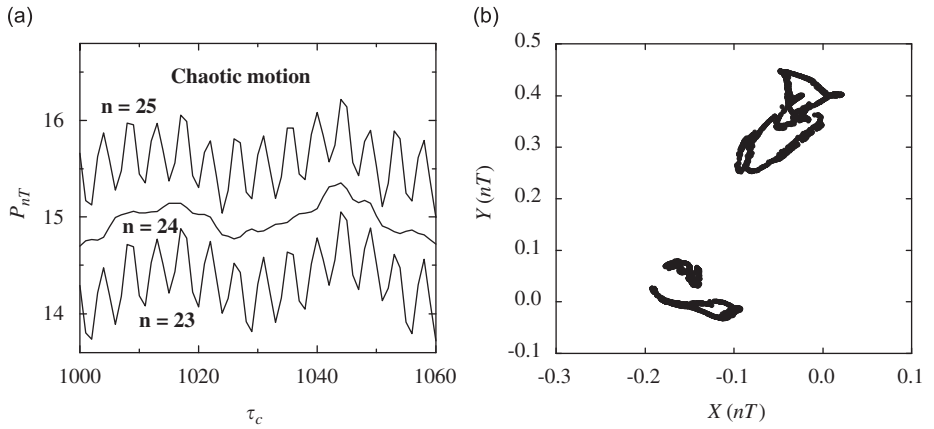

Fig. 7. (a) The response integration value plot and (b) Poincaré map with rotating speed ratio, $\Omega = 2.7925$.

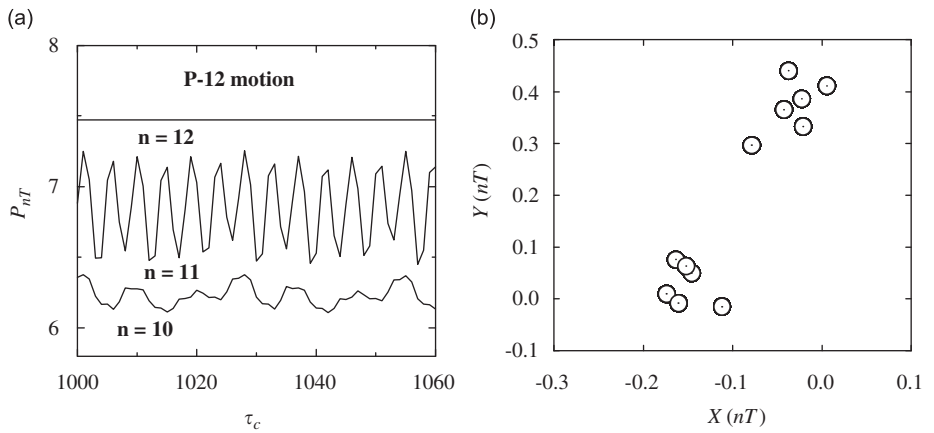

Fig. 8. (a) The response integration value plot and (b) Poincaré map with rotating speed ratio, $\Omega = 2.80$.

vibration with period six from Fig. 5(b). As the rotating speed ratio continues to increase; the periodic motion loses stability and then another region of chaos appears. It is found that the response integration value never keeps constant as continuously varying τ_c even with the integration interval set very large ($n = 23$ and 25) as shown in Figs. 6(a) and 7(a). It indicates that responses are not periodic motions. The results of the Poincaré section method also show the responses to be chaotic motions. When the rotating speed ratio is 2.8, the chaotic motion disappears and becomes a periodic vibration again as shown in Fig. 8(b). Similarly, it is also difficult to identify periodic responses; this is due to some Poincaré section points being too close. But we can easily observe is that the motion is a sub-harmonic vibration with period 12 as shown in Fig. 8(a). It can be seen that the rub-impacting rotor system represents the complex dynamic characters at different rotating speeds obviously.

Figs. 9–12 show the Poincaré maps and response integration value plots with various initial vertical eccentric ratios of 0.70, 0.77, 0.86 and 0.95, respectively, where $K = 0.033$, $\xi = 0.10$, $\Delta X = 0.5$, $U = 0.12$, $\mu = 0.2$, $\Omega = 2.6$. In the analysis of the Poincaré section method, the extraction time equals to the external excitation period of $T = 2\pi/\omega$. When the vertical eccentric ratio is 0.70, there are four points in the Poincaré map as shown in Fig. 9(b). Therefore, the system response is a period four motion. The result is the same as the one of the response integration method as shown in Fig. 9(a). At $\Delta Y = 0.77$, due to a few Poincaré section points being too close, it is difficult to identify the periodic response of the sub-harmonic vibration as shown in Fig. 10(b). But from Fig. 10(a), the response integration value plot, we can differentiate the motion clearly to be a sub-harmonic vibration with period sixteen. As ΔY is increased to 0.86, it is found that the P_{nT} integration value never keeps constant as continuously varying τ_c even with the integration interval set very large as shown in Fig. 11(a). The result of the Poincaré section method also shows the response to be chaotic motion as shown in Fig. 11(b). When the initial vertical eccentric ratio ΔY reaches 0.95, the Poincaré section points appear to fill up a closed curve as shown in Fig. 12(b). Then the motion becomes quasi-periodic. At this time, the ΔP_{nT} integration value never keeps constant as continuously varying τ_c even with the integration interval set very large ($n = 30$) as shown in Fig. 12(a).

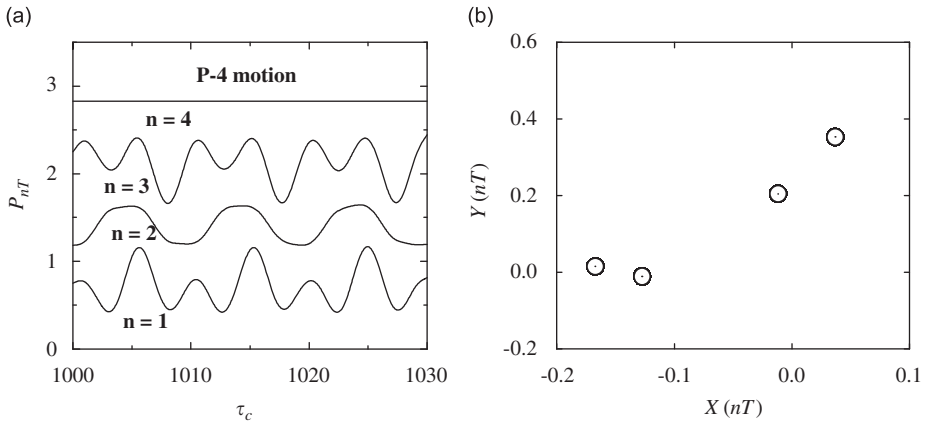

Fig. 9. (a) The response integration value plot and (b) Poincaré map with initial eccentric ratios, $\Delta Y = 0.70$.

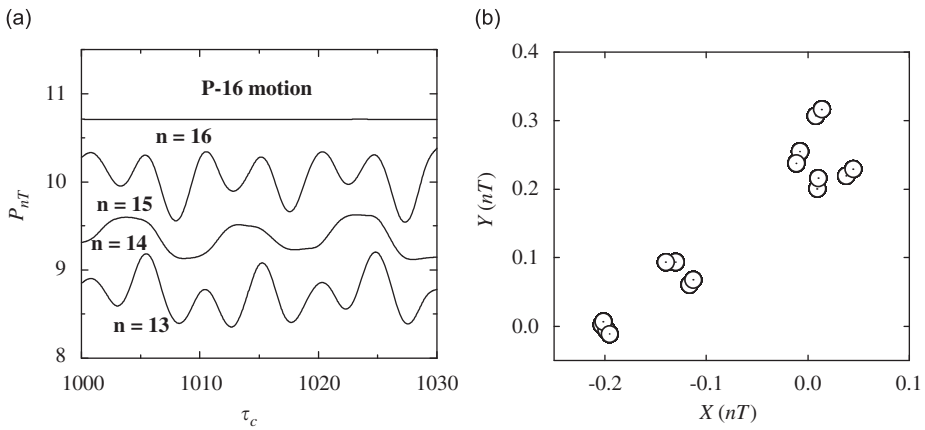

Fig. 10. (a) The response integration value plot and (b) Poincaré map with initial eccentric ratios, $\Delta Y = 0.77$.

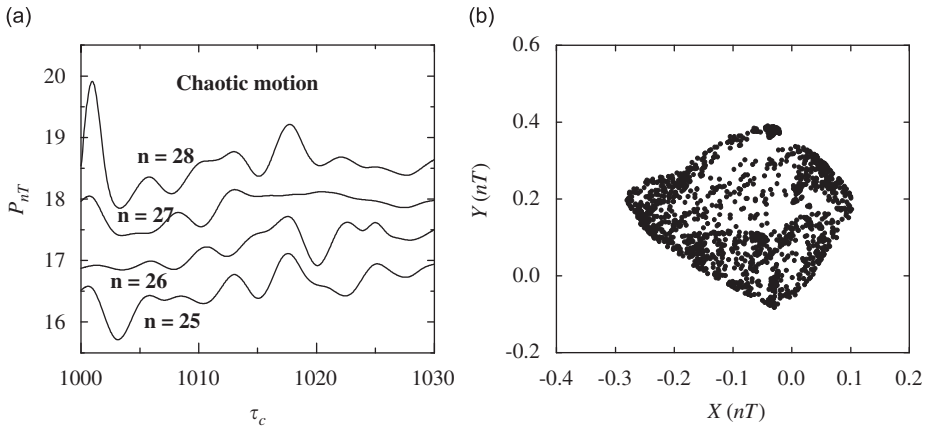

Fig. 11. (a) The response integration value plot and (b) Poincaré map with initial eccentric ratios, $\Delta Y = 0.86$.

4.2. Bifurcation diagram of rub-impacting rotor

The bifurcation diagram is a very effective mean to reflect the motion change; the results obtained from the system exhibiting of nonlinear behaviors may be presented. In order to compute a bifurcation diagram, a control parameter was varied at a constant step. The initial eccentric measure of a rotor is a very important parameter which is related to the

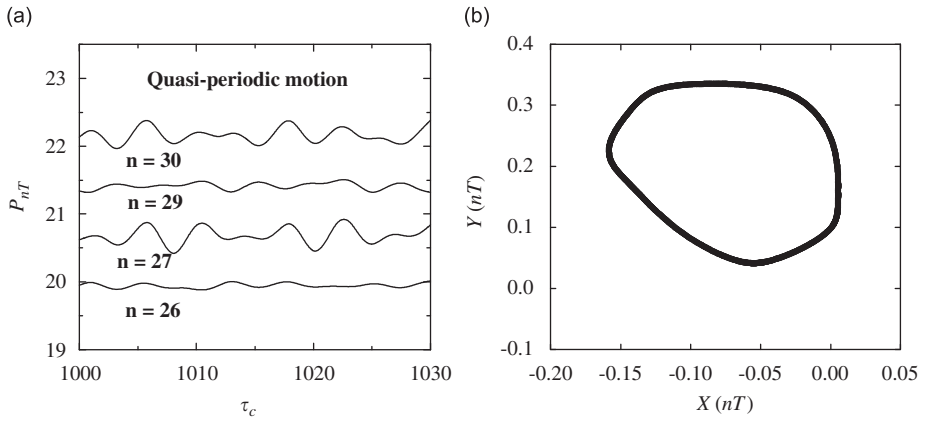

Fig. 12. (a) The response integration value plot and (b) Poincaré map with initial eccentric ratios, $\Delta Y = 0.95$.

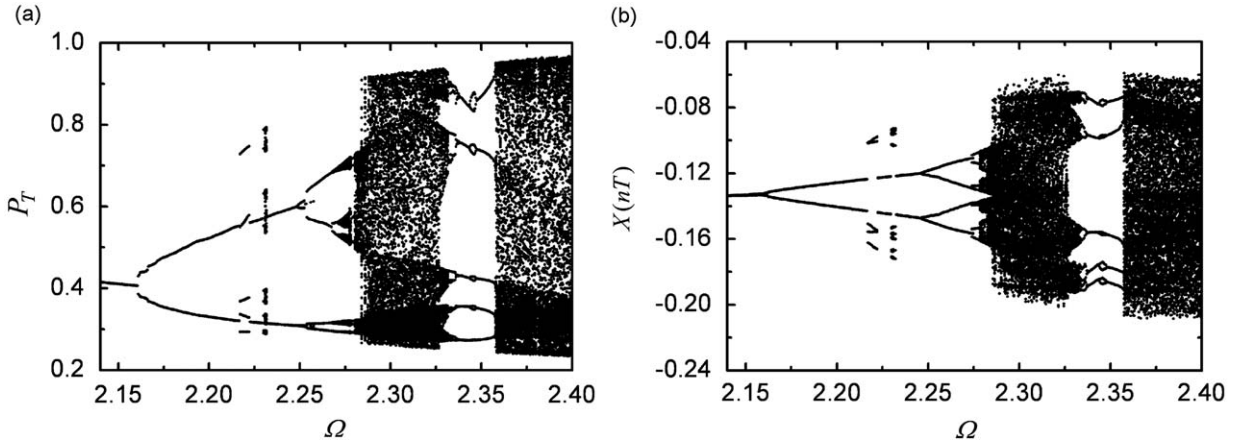

Fig. 13. Bifurcation diagrams with rotating speed ratio, Ω as the control parameter: (a) the response integration method and (b) Poincaré section method, where $K = 0.034$, $\xi = 0.10$, $\Delta X = 0.0$, $\Delta Y = 0.9$, $U = 0.1$, and $\mu = 0.2$.

stability of rotor motion directly. In order to validate the analysis results from the response integration method, comparisons are made with Poincaré section method. Figs. 13(a) and (b) are the bifurcation diagrams drawn with both the response integration method and the Poincaré section method, using the rotating speed ratio as the control parameters. The rotating speed ratio Ω ranges from 2.14 to 2.4 with a step of 0.0005. It can be seen that the response integration method and the Poincaré section method almost show the same topology of the structure for the same rotor's parameters. Similarly, the present method is evaluated by a comparison with Poincaré section method to show the excellent agreement. The Rotor's imbalance plays an important part in the behavior of the system. In a turbine or compressor, the sudden loss of blade will increase the imbalance and results in rubbing. Figs. 14(a) and (b) are the bifurcation diagrams drawn with both the Poincaré section method and the response integration method, using the imbalance as the control parameters. Overall the results obtained from the Poincaré section method were comparable with those from the response integration method. These similarities validated the numerical model. As the simulated results were broadly similar to those from the response integration method, further numerical simulations were undertaken to investigate the effect on the response of the system. Here the effect of increasing the imbalance, from 0.065 to 0.085, is investigated. The bifurcation diagram shows that a further increase imbalance causes the onset of subharmonic motions of various orders, interspersed with chaotic bands. At $U = 0.065$ a period two motion exists at first, and then at about $U = 0.068$ the motion becomes period four. When imbalance increases further, the response exists periodic motion and turns into chaotic motion at $U = 0.0705$. Increasing imbalance will result in rubbing and induce nonsynchronous responses. This feature indicates that the imbalance effect is relatively sensitive to the dynamic responses of a rotor system.

Damping is also one of the main factors affecting dynamic characteristics of nonlinear systems. Bifurcation diagrams shown in Fig. 15 was plotted in the form of P_T integration to be as a function of the U with the variation of damping parameter ξ. In the range $0.06 < U < 0.1$, the bifurcations of the system are illustrated for damping parameters ξ of 0.08, 0.10, 0.12 and 0.15. As obvious from bifurcation responses shown in Fig. 15, increasing ξ can reduce the response amplitude

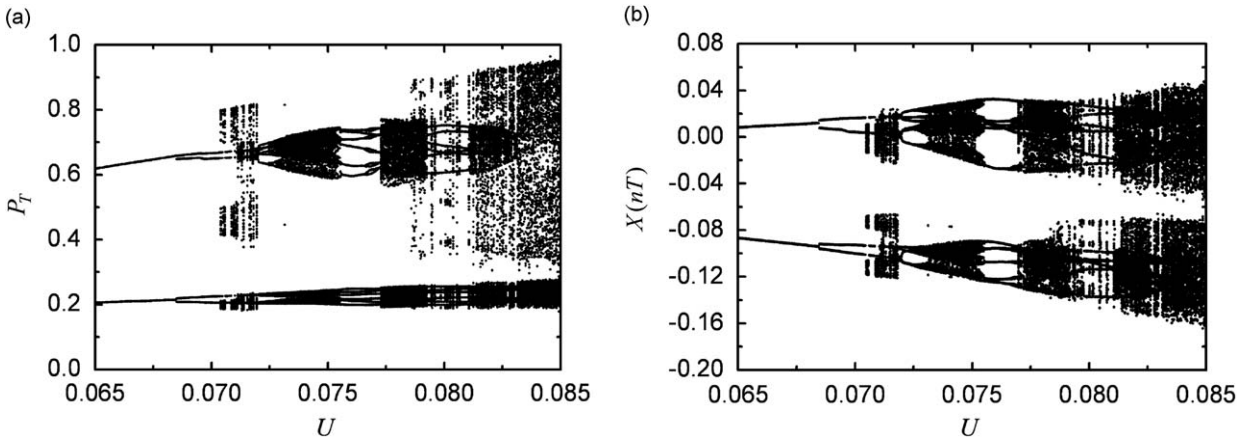

Fig. 14. Bifurcation diagrams with imbalance ratio, U as the control parameter: (a) the response integration method and (b) Poincaré section method, where $K = 0.032$, $\Delta X = 0.5$, $\Delta Y = 0.8$, $\mu = 0.2$, and $\Omega = 2.6$.

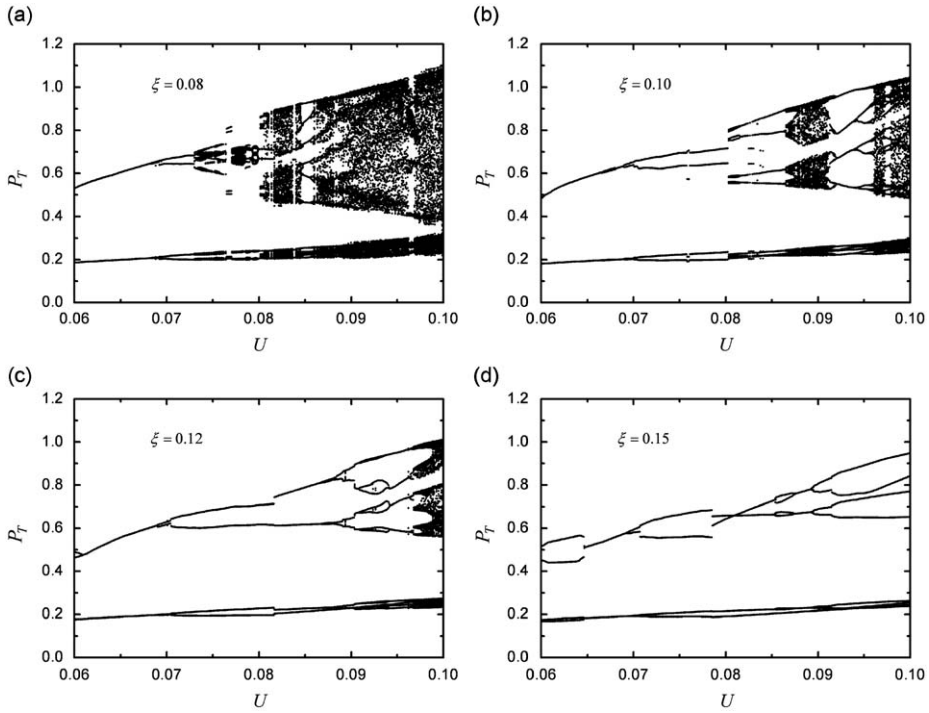

Fig. 15. Effect of damping coefficient, ξ on the system responses of bifurcation diagrams using the response integration method, where $K = 0.032$, $\Delta X = 0.5$, $\Delta Y = 0.8$, $\mu = 0.2$, and $\Omega = 2.6$.

and narrows the chaotic zone. It is further observed that as the value of ξ is increased from 0.08 to 0.15. The chaotic zones gradually disappear. For the case of $\xi = 0.10$, the chaotic zone in the half-right interval, i.e., $0.08 < U < 0.1$ was also narrowed in Fig. 15(b). For the case of $\xi = 0.15$ in particular, the chaotic zones entirely disappear in Fig. 15(d). It can be seen that the system represents the complex dynamic characters at different damping coefficients obviously. The chaotic zones gradually disappear when the damping parameter is increased. This feature indicates that the damping effect is relatively sensitive to the dynamic responses of a system. The effect of changing stiffness parameter is also investigated in this paper.

Bifurcation diagrams shown in Fig. 16 was plotted in the form of P_T integration to be as a function of the U with various stiffness parameters K. For a lower stiffness value of $K = 0.036$, it is clearly seen that there are several chaotic regions occur in the range $0.072 < U < 0.1$. As obvious from bifurcation responses shown in Figs. 16(a)–(d), increasing K also reduces the response amplitude and narrows the chaotic zone. It is observed that as the value of K is increased from 0.036 to 0.045, the chaotic zones gradually decrease. When K increases further, at $K = 0.04$ as shown in Fig. 16(c) the chaotic regions are found

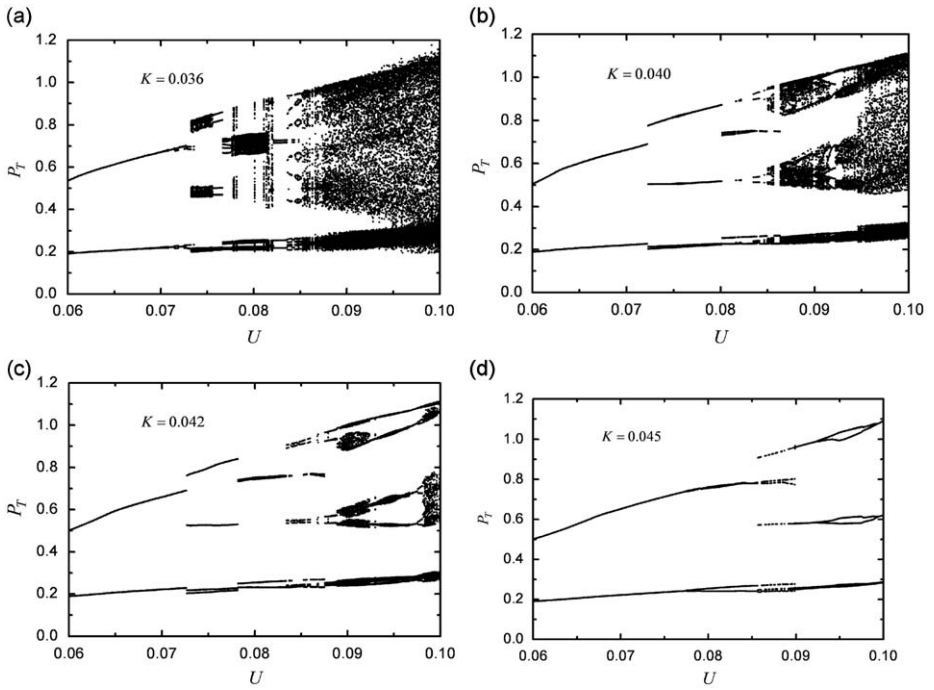

Fig. 16. Effect of stiffness coefficient, K on the system responses of bifurcation diagrams using the response integration method, where $\xi = 0.06$, $\Delta X = 0.5$, $\Delta Y = 0.8$, $\mu = 0.2$, $\Omega = 2.6$.

to be narrowed. Then, with further variations of K, Fig. 16(d) shows that the chaotic zones disappear and the level of vibration is lower when the stiffness is larger (at $K = 0.045$).

5. Conclusions

To apply the effective methods to analyze and distinguish all kinds of response patterns is the major research object of nonlinear dynamics. The dynamic equations of a rotor system with rub-impact are obtained and solved numerically. This study proposes an integration algorithm to analyze the vibration responses of a rotor system with rub-impact. With utilizing the integration algorithm, the response patterns of the system can be clearly and simply drawn and avoid the misjudgment. It provides a quantitative characterization of system responses and can assist the role of the Poincaré section method to observe bifurcations and chaos of the nonlinear system. For a high-order harmonic vibration, the system responses will be made misjudgments due to the Poincaré section points near each other. However, when the integration value is a fixed constant, the system response is a periodic motion which is based on the definition of the response integration method. In this paper we have inspected the P_{nT} integration plot and P_T integration bifurcation diagram to identify responses of a rubbing rotor system. It is more advantageous to use this method for analysis regarding limited measuring data or numerical simulation. Applying this response integration, the effects of the change in the stiffness and the damping coefficients on the vibration features of a rubbing rotor system are investigated. From simulation results, it shows that the responses of a rubbing rotor exhibit very complicated types of higher subharmonic oscillation, period-doubling bifurcation and chaotic motions.

Acknowledgment

This research had been supported by a grant from the National Science Council of R.O.C. under Contract NSC89-TPC-7-033-008.

References

[1] D.W. Childs, Rub-induced parametric excitation in rotors, *American Society of Mechanical Engineers Journal of Mechanical Design* 101 (1979) 640–644.
[2] D.W. Childs, Fractional frequency rotor motion due to nonsymmetrical clearance effects, *Journal of Energy and Power* 104 (1982) 533–541.
[3] R.F. Beatty, Differentiating rotor response due to radial rubbing, *Journal of Vibration, Acoustics, Stress, and Reliability in Design* 107 (1985) 151–160.
[4] F.K. Choy, J. Padovan, Non-linear transient analysis of rotor-casing rub events, *Journal of Sound and Vibration* 113 (1987) 529–545.

[5] Y.S. Choi, S.T. Noah, Nonlinear steady-state response of a rotor support system, *Journal of Vibration, Acoustics, Stress, and Reliability in Design* 109 (1987) 255–261.
[6] F.F. Ehrich, High order sub-harmonic response of high speed rotors in bearing clearance, *Journal of Vibration, Acoustics, Stress, and Reliability in Design* 110 (1988) 9–16.
[7] F.F. Ehrich, Observations of subcritical superharmonic and chaotic response in rotor dynamics, *Journal of Vibration, Acoustics, Stress, and Reliability in Design* 114 (1992) 93–100.
[8] P. Goldman, A. Muszynska, Dynamic effects in mechanical structures with gaps and impacting: order and chaos, *Journal of Vibration and Acoustics* 116 (1994) 541–547.
[9] P. Goldman, A. Muszynska, Chaotic responses of unbalanced rotor/bearing/stator systems with looseness or rubs, *Chaos, Solitons and Fractals* 5 (1995) 1683–1704.
[10] F. Chu, Z. Zhang, Periodic, quasi-periodic and chaotic vibrations of a rub-impact rotor system supported on oil film bearings, *International Journal of Engineering Science* 35 (1997) 963–973.
[11] F. Chu, Z. Zhang, Bifurcation and chaos in a rub impact Jeffcott rotor system, *Journal of Sound and Vibration* 210 (1998) 1–8.
[12] S. Edwards, A.W. Lees, M.I. Friswell, The influence of torsion on rotor/stator contact in rotating machinery, *Journal of Sound and Vibration* 225 (1999) 767–778.
[13] Z.C. Feng, X.Z. Zhang, Rubbing phenomena in rotor-stator contact, *Chaos, Solitons and Fractals* 14 (2002) 257–267.